

PAPER

PD sliding mode control of active suspension based on adaptive disturbance observer

To cite this article: Zhonghui Sun *et al* 2025 *Meas. Sci. Technol.* **36** 076211

View the [article online](#) for updates and enhancements.

You may also like

- [Generalized differentiable Perspective-n-Point without 2D-3D correspondences for pose measurement](#)
Huabo Zhu, Yuzhao Chen, Bowen Liang et al.
- [A novel framework for the uncertainty evaluation of virtual flow meters](#)
Nursen Bayazit, Manuel Marschall, Martin Straka et al.
- [Design and experimental characterization of a small flexible TMR-based indentation probe for soft tissue hardness estimation](#)
Giacomo Santona, Antonio Fiorentino, Francesco Doglietto et al.

The advertisement features the ECS logo and the text "The Electrochemical Society Advancing solid state & electrochemical science & technology". On the left, there's a circular logo for "SUSTAINABLE TECHNOLOGIES" with a stylized globe and leaves. Below it, the text reads: "249th ECS Meeting May 24-28, 2026 Seattle, WA, US Washington State Convention Center". On the right, the text "Spotlight Your Science" is displayed prominently in white, with a "Submission deadline: December 5, 2025" below it. A green button at the bottom right says "SUBMIT YOUR ABSTRACT".

PD sliding mode control of active suspension based on adaptive disturbance observer

Zhonghui Sun^{ID}, Sujuan Shao^{*}^{ID}, Zhongwei Zhang, Jiangduo Liu^{ID}, Hao Tang, Liangjie Li and Shipeng Yuan

School of Transportation and Vehicle Engineering, Shandong University of Technology, Zibo 255000, People's Republic of China

E-mail: ssjsdut@sdut.edu.cn

Received 17 March 2025, revised 22 June 2025

Accepted for publication 2 July 2025

Published 11 July 2025



Abstract

The control efficacy of active suspension systems is influenced by inherent nonlinearities, uncertainties in the sprung mass, and external disturbances. To address these challenges, this study proposes a proportional-derivative sliding mode controller integrated with an adaptive disturbance observer (ADO). The proposed ADO offers significant advantages, primarily due to its capability to significantly attenuate high-frequency oscillatory behavior commonly associated with conventional fixed-gain observers, while eliminating the need for *a priori* information regarding disturbance magnitude bounds or their rate of change. Furthermore, the robustness of the ADO is substantially improved, enabling it to effectively counteract a wide range of disturbances. Additionally, recognizing the dual nature of disturbances—where they can exhibit both advantageous and adverse effects—a disturbance effect indicator (DEI) is developed. By leveraging the adaptive estimation mechanism of the ADO in conjunction with the DEI, detrimental disturbances are actively mitigated, while beneficial components are preserved and utilized. The input-to-state stability of the developed active suspension control framework is analytically established via Lyapunov-based stability criteria. Experimental validation under standardized road excitation scenarios confirms the controller's performance efficacy, with root-mean-square chassis acceleration reduced by 67.67% and 52.54% compared to passive configurations under bump and random road excitation profiles, respectively.

Keywords: active suspension system, disturbance observer, disturbance effect indicator, sliding mode control

1. Introduction

Suspension systems are regarded as critical components of automobiles, with their pivotal role being the enhancement of vehicle handling stability, ride comfort, and driving smoothness [1, 2]. Suspension systems are divided into three types—passive, semi-active, and active—depending on their structural configurations [3]. Compared to passive and semi-active suspension systems, active suspension systems

are widely acknowledged for their superior ride comfort and road handling performance when irregular road surfaces are encountered by vehicles. This is primarily attributed to the integration of additional actuators, which facilitate more efficient energy distribution.

The performance of active suspension systems relies on advanced control algorithms to dynamically modulate suspension stiffness and damping characteristics, facilitating real-time adaptation to diverse road profiles and driving demands [4]. Consequently, the design and optimization of these control strategies are critical determinants of both system stability and ride comfort. With the continuous advancement

* Author to whom any correspondence should be addressed.

of active suspension technology, the design of efficient and robust control strategies has become a focal point of research in recent years [5, 6]. Considering the nonlinear spring and damping characteristics of the suspension system, model uncertainties, and road disturbances, it is crucial to design a controller to ensure the system's stability and robustness under these highly uncertain conditions.

In recent years, various represent active control methods have been proposed by scholars to address nonlinearities and parameter uncertainties in active suspension systems, including robust control [7, 8], fuzzy control [9, 10], neural network control [11], and sliding mode control [12, 13]. In [14], robust state feedback control is utilized to address suspension systems with parameter uncertainties. However, this method is unable to ensure passenger comfort and driving safety [15]. To address this issue, a parametric multi-objective robust control method is proposed in [16], which optimizes system performance by adjusting the controller's parameter values. This approach is not only straightforward to implement but also capable of balancing comfort and safety to a certain extent. In [17], an adaptive inverse control method was proposed, demonstrating superior performance in enhancing passenger com-fort and particularly effective in addressing complex road surface variations and driving conditions. To circumvent the complexity associated with identifying the dynamic parameters of the suspension system, fuzzy logic control was integrated with neural network control in [18–20]. In this approach, fuzzy logic is employed to handle uncertainties, while neural networks are utilized to approximate unknown functions. However, this method involves many learning parameters, which increases the complexity and computational burden of system implementation, thereby limiting its widespread adoption in practical applications [21].

Sliding mode control, a well-known robust control technique, is widely applied due to its significant advantages of fast convergence and strong robustness to disturbances and uncertainties [22]. Several researchers have utilized it to address various issues in active suspension systems. To address the nonlinearities of active suspension elements, a terminal sliding mode control method is proposed in [23], which achieves accurate tracking of vehicle attitude and significant improvement in ride comfort. In [24], a fractional-order terminal sliding mode control strategy is proposed to reduce the head acceleration of both the driver and passengers. Leveraging the independent adjustability of PD control gains and the capability of the PD component to partially replace the equivalent control in sliding mode control, a PD-based sliding mode control method is developed in [25, 26] and applied to suspension systems, thereby eliminating the need for calculating the equivalent control term.

Interference observation and compensation control technologies have been widely applied in complex mechanical systems, particularly in scenarios involving unmodeled dynamics and uncertain disturbances [27]. In recent years, the use of disturbance observers to address uncertainties and disturbances in control systems has become a research hotspot [28]. Some researchers have integrated sliding mode control with disturbance observers to mitigate the effects of unknown

parameters within the system. In [29], a sliding mode control method based on a linear disturbance observer is proposed to address issues such as deterministic and non-ideal actuators. However, the problem of actuator saturation is not considered in [29], which may result in a significant degradation of control performance. To address this issue, a nonlinear disturbance compensation design method is proposed in [30], which effectively prevents actuator saturation, thereby avoiding performance deterioration and extending the operational lifespan of the actuator.

In the presence of parameter uncertainties, external disturbances, and system nonlinearities in pneumatic active suspension systems, an adaptive sliding mode controller based on a nonlinear disturbance observer is proposed in [31]. In [32], a sliding mode controller integrated with a disturbance observer is proposed to address the issue of suspension deflection failing to converge to zero within a finite time under nonlinearities and disturbances in active suspension systems. By incorporating the ceiling damping model, the phenomenon of the suspension impacting the limit block is effectively avoided. However, the design parameters of the aforementioned observers typically depend on upper-bound information about the disturbance or its derivative, which is often unknown or difficult to obtain in practical applications. To address this limitation, a two-layer adaptive law for disturbance observation is proposed in [33], which eliminates the need for upper-bound information about the disturbance derivative but still requires knowledge of the upper-bound information of the second derivative. In addition, traditional disturbance observer-based control methods face the issue that the estimation error cannot converge to zero or a bounded set within a finite time. To address this problem, an adaptive sliding mode disturbance observer is introduced in [34]. Based on this observer, the disturbance estimation error can converge to a bounded set in finite time without requiring the upper-bound information of the disturbance derivative. However, this method assumes that the upper bound of the disturbance is known and does not account for unmodeled dynamics and external disturbances.

On the other hand, existing robust control methods typically treat disturbances as detrimental factors and aim to eliminate them. However, disturbances possess a dual nature: they may adversely affect the system or positively contribute to its performance. Therefore, while it is essential to eliminate harmful disturbances, indiscriminately removing all disturbances may inadvertently eliminate those that are beneficial to the system, thereby compromising its overall performance. For this reason, a DEI is proposed in the literature [35–37]. Compared to traditional disturbance suppression methods, the DEI can more effectively distinguish the different characteristics of disturbances, thereby avoiding the risk of indiscriminately suppressing beneficial disturbances. This approach enhances the vehicle's tracking accuracy and transient response performance. Based on this concept, the disturbance effect indicator (DEI) based on symbolic functions was applied to suspension systems in [38, 39]. By effectively utilizing beneficial disturbances, the transient response performance of the system was significantly improved, and the efficiency of control energy utilization was also optimized. However, although the

DEI based on symbolic functions can enhance the system's robustness, in practical applications when the tracking error approaches zero, chattering may occur due to rapid changes in the direction of the error.

Based on the above analysis, this paper proposes a new composite control scheme to address the impact of nonlinearity and uncertain parameters in a quarter-active suspension system. The proposed control method outperforms traditional passive suspension, SPD-SMC active suspension, and SMC-DO active suspension in terms of control performance and robustness to uncertain parameters. The main contributions are as follows:

1. The nonlinearities of the active suspension system, the uncertainty of the sprung mass, and external disturbances are integrated into a unified concentrated disturbance. Based on this framework, an adaptive disturbance observer (ADO) is introduced, capable of estimating the concentrated disturbance without the need for upper-bound information of the disturbance or its derivatives, while ensuring that the estimation error converges to a bounded range within finite time.
2. A new method for condition-based disturbance compensation is designed to effectively evaluate the disturbances compensated by the disturbance observer. This method includes a disturbance characteristic indicator (DCI) and a switching logic function (SLF), which can eliminate harmful disturbances while retaining beneficial ones.
3. A novel composite control scheme is proposed by combining the proportional-derivative sliding mode controller with a new ADO. The proposed control method not only exhibits robust performance against uncertain disturbances but also avoids the chattering issues caused by high disturbance estimation values.

The structure of this article is organized as follows. Section 2 outlines the control problem under consideration. In Section 3, the control strategy is elaborated, including the development of the ADO, the DEI, the PD sliding mode control approach, and the stability analysis of the closed-loop system. Section 4 provides experimental results to demonstrate the enhanced control performance of the proposed tracking controller. The half-vehicle model simulation is described in section 5. Finally, section 6 summarizes the entire study.

2. System description and requirements

Figure 1 illustrates a quarter-car suspension model that includes unknown parameters and disturbance factors. This two-degree-of-freedom system is commonly found in the literature [25]. The dynamic equations describing the motion of the quarter-car suspension system are as follows:

$$\begin{cases} m_s \ddot{z}_s = -F_s - F_d + u + d_1 \\ m_u \ddot{z}_u = F_s + F_d - F_t - F_b - u + d_2 \end{cases} \quad (1)$$

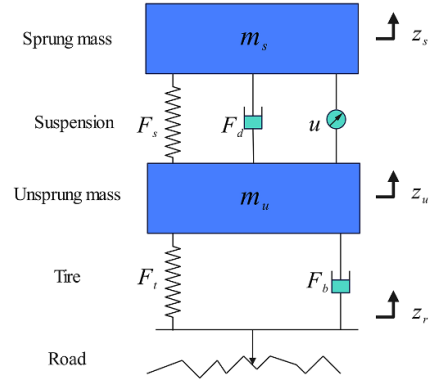


Figure 1. Structure of a quarter-vehicle active suspension system.

where m_s and m_u are the sprung mass and unsprung masses, respectively; z_s and z_u refer to the vertical displacements of the sprung and unsprung masses, respectively; z_r represents the vertical displacement of the road input; d_1 and d_2 represents the disturbance, including unmodeled/uncertain dynamics and external disturbances; F_s and F_d are the forces produced by the nonlinear spring and nonlinear damper of the suspension components, respectively; F_t and F_b represent the elasticity and damping forces of the tire, respectively. u represents the control input;

The mathematical equations describing the output forces of the suspension components and the tire are formulated as follows:

$$\begin{cases} F_s(z_s, z_u) = k_s(z_s - z_u) + k_{sl}(z_s - z_u)^3 \\ F_d(\dot{z}_s, \dot{z}_u) = c_s(\dot{z}_s - \dot{z}_u) + c_{sl}(\dot{z}_s - \dot{z}_u)^2 \\ F_t(z_u, z_r) = k_t(z_u - z_r) \\ F_b(\dot{z}_u, \dot{z}_r) = c_t(\dot{z}_u - \dot{z}_r) \end{cases} \quad (2)$$

where k_s , k_{sl} , c_s , and c_{sl} denote the stiffness and damping coefficients of the suspension components, respectively; k_t and c_t represent the stiffness and damping coefficients of the tire.

Due to the limitations of the vehicle structure and actual physical properties, the sprung mass m_s can be rewritten as nominal mass m_{s0} and uncertain mass Δm_{s0} [26–31],

$$m_s = m_{s0} + \Delta m_{s0}. \quad (3)$$

In practical applications, the springs and dampers in suspension systems often exhibit nonlinear characteristics, and the coefficients of these nonlinear terms are generally unknown [11]. Accurately determining these nonlinear coefficients is challenging, and their impact on the system is complex. Therefore, these nonlinear effects are simplified and treated as unknown disturbances for analytical purposes. Consequently, the equation (1) is reformulated as follows:

$$m_{s0} \ddot{z}_s = D + u \quad (4)$$

where D represents the lumped disturbance of the system. The specific expression is provided below:

$$D = d_1 - \Delta m_s \ddot{z}_s - F_s - F_d. \quad (5)$$

For active suspension systems, improving vehicle ride comfort is the core performance metric of the control strategy. This metric is typically evaluated by measuring the acceleration of the sprung mass, including its root mean square (RMS) value, with the specific calculation method provided in the following mathematical equations,

$$\text{RSM} \|\ddot{z}_s\| = \frac{1}{T} \int_0^T \ddot{z}_s^2 dt. \quad (6)$$

Reasonable deflection limits can not only prevent mechanical damage to the suspension system caused by excessive compression or extension but also ensure the stability and safety of the vehicle under various operating conditions. Here, MRSD denotes the maximum allowable limit of suspension deflection,

$$\text{MRSD} = \frac{|z_s - z_u|_{\max}}{z_{\max}}. \quad (7)$$

Maximum relative tire deflection (MRTD) refers to the deformation or shape change of the tire due to external forces, particularly under conditions such as uneven road surfaces or impacts. This parameter is critical for ensuring the suspension system's performance and the vehicle's overall stability,

$$\text{MRTD} = \frac{|z_u - z_r|_{\max}}{t_{\max}}. \quad (8)$$

where $t_{\max} = (m_s + m_u)g/3k_t$ is the maximum tire deflection, and k_t denotes the tire stiffness.

Remark 1. MRSD and MRTD are critical indicators for evaluating the safety and road-holding capability of a suspension system. It is essential to ensure that the amplitude of MRSD remains below 1 to guarantee that the suspension system operates within its spatial constraints. Furthermore, to maintain effective tire-to-ground contact and ensure optimal road-holding performance, the amplitude of MRTD must also be maintained below 1.

The following lemma is used throughout the rest of this article.

Lemma 1 ([40]): Consider system (4), assuming standard constants $c > 0$ and $0 < \varsigma < 1$ exist such that the continuous positive definite function $V(x)$ satisfies $\dot{V}(x) \leq -c(V(x))^\varsigma$. Therefore, the system is finite-time stable, and the reaching time is bounded by the following equation,

$$T \leq \frac{1}{c(1-\varsigma)} (V(0))^{1-\varsigma} \quad (9)$$

where $V(0)$ is the initial value of $V(x)$.

Lemma 2 ([41]): If there exists $\Omega \in R^n$ continuously differentiable positive definite function $V(x) > 0$ and $V(0) = 0$ in a neighborhood a containing the origin, along with real numbers $0 < \theta < 1$, and $\vartheta > 0$ such that $\dot{V}(x)$ satisfies the condition $\dot{V}(x) \leq -\vartheta V^\theta(x) + o$, then the system state $x(t)$ will converge to a neighborhood around the origin after a finite time t_0 , that is, at time $t \geq t_0$,

$$V^\theta(x) \leq \frac{\sigma}{(1-\theta_0)\Gamma}, 0 < \theta_0 < 1 \quad (10)$$

$$t_0 = \frac{V^{1-\theta}(x_0)}{\vartheta\theta_0(1-\theta)} \quad (11)$$

where is the initial state of the system x_0

3. Control scheme

3.1. Two-layer ADO

This section introduces an ADO aimed at achieving accurate estimation and efficient mitigation of combined disturbances. The observer incorporates an adaptive framework, and stability analysis reveals that estimation errors can be confined to a bounded set within a finite duration. In comparison to conventional approaches, the proposed observer provides distinct benefits: it dynamically adjusts to disturbance variations without necessitating prior information about disturbance limits or their derivatives in the design stage.

Defining the sliding variable

$$s = \dot{z}_s - \eta \quad (12)$$

where η is the auxiliary variable.

To design the observer, the following auxiliary variables are introduced,

$$m_s \dot{\eta} = u + \hat{D} + \lambda_0 s + v \quad (13)$$

where \hat{D} represents the estimated value of the lumped disturbance D in system (4). The scalar λ_0 is the gain of the auxiliary variable, and $v = (h(t) + \bar{\delta}) \operatorname{sgn}(s)$, where $\bar{\delta}$ is a normal constant, and $h(t)$ will be designed later. The observer estimation error is defined as $\tilde{D} = D - \hat{D}$.

Assumption 1 [39, 42]: The lumped disturbance D described in the system (4) and the derivative of the lumped disturbance \dot{D} satisfy:

$$|D| < \beta_1, |\dot{D}| < \beta_2 \quad (14)$$

where $\beta_1 > 0, \beta_2 > 0$ are all unknown constants.

From (4), (12) and (13), we have

$$m_s \dot{s} = \tilde{D} - \lambda_0 s - v \quad (15)$$

where l is an unknown constant, and $|\dot{\tilde{D}}| < l$. An adaptive structure was used in [43, 44], which does not require the upper bound information of the disturbance and its derivatives, yet

the system (15) can still reach the sliding surface. Therefore, the following adaptive structure is used to update $h(t)$ in system (15),

$$\dot{h}(t) = -(r_0 + r(t)) \operatorname{sgn}(\delta(t)) \quad (16)$$

$$\dot{r}(t) = \begin{cases} \mu |\delta(t)| & |\delta(t)| > \delta_0 \\ 0 & |\delta(t)| \leq \delta_0 \end{cases} \quad (17)$$

$$\delta(t) = h(t) - \frac{|\chi(t)|}{\alpha_1} - \alpha_2 \quad (18)$$

$$\dot{\chi}(t) = \frac{1}{\tau}(-v - \chi(t)) \quad (19)$$

where $r_0, \mu, \delta_0, 0 < \alpha_1 < 1, \alpha_2$ and τ are the normal constants to be designed. They should satisfy the following conditions:

$$\frac{1}{4}\alpha_2^2 > \delta_0^2 + \frac{1}{\mu} \left(\frac{ql}{\alpha_1} \right)^2 \quad (20)$$

q is the safety margin, which satisfies $q > \sup(1, |\dot{\chi}|/l)$. The parameter l in inequality (20) does not need to be precisely known. By choosing a sufficiently large μ , it is possible to ensure the existence of a constant α_2 such that inequality (20) holds [45].

Based on Assumption 1, the unknown constant β_2 is employed to denote the upper bound of \tilde{D} , which is not available in advance. The ADO can be formulated as follows:

$$\begin{cases} \hat{D} = z + \lambda_1 m_{s0} \dot{z}_s \\ \dot{z} = -\lambda_1 (u + \hat{D}) + (\hat{\beta}_2 + \lambda_2) \operatorname{sgn}(v) \\ \dot{\hat{\beta}}_2 = -\lambda_3 \hat{\beta}_2 + |v| \end{cases} \quad (21)$$

where λ_1, λ_2 , and λ_3 are positive constants serving as the observer gains, z is an intermediate variable, and $\hat{\beta}_2$ is the estimated value of the upper bound of the lumped disturbance derivative β_2 .

3.2. Stability analysis

Theorem 1. Based on Assumption 1, the adaptive observer (21) developed for system (4) guarantees that the observation error \tilde{D} converges to a vicinity of the origin within a finite time frame.

Proof. Firstly, it will be shown that the sliding variable s in (15) converges to the origin in finite time under the adaptive structure (16)–(19).

Choose the Lyapunov function V_1

$$V_1 = \frac{1}{2} m_{s0} s^2. \quad (22)$$

By differentiating the equation concerning the equation (15), we obtain:

$$\begin{aligned} \dot{V}_1 &= s(\tilde{D} - \lambda_0 s - (h(t) + \bar{\delta}) \operatorname{sgn}(s)) \\ &\leq -\lambda_0 s^2 + \tilde{D} |s| - h(t) |s| - \bar{\delta} |s| \\ &\leq -|s|(h(t) - |\tilde{D}|) - \bar{\delta} |s| \end{aligned} \quad (23)$$

As indicated in [45], the condition $h(t) > l > |\tilde{D}|$ can be satisfied within a finite time t_0 , and $h(t)$ remains bounded. Specifically, there exists a constant $M > 0$ such that $|h(t)| \leq M$ holds. Consequently, the equation can be reformulated as follows:

$$\dot{V}_1 \leq -\frac{\bar{\delta}}{\sqrt{m_{s0}}} V_1^{1/2}. \quad (24)$$

Based on Lemma 1, the sliding variable s converges to $s = 0$ within a finite time $t_1 \leq (m_{s0}/\bar{\delta}) V_1^{1/2}(t_0)$. When $\dot{s} = 0$, it follows from equation (15) that the estimation error \tilde{D} equals v , i.e. $\tilde{D}_{\text{eq}} = v$. The subscript ‘eq’ denotes the equivalent state where the sliding variables satisfy $s = \dot{s} = 0$.

Next, we will prove that after, under the adaptive observer, the estimation error \tilde{D} will converge to a bounded region near the origin within a finite time.

Subsequently, it will be demonstrated that after $s = \dot{s} = 0$, the estimation error \tilde{D} converges to a bounded region near the origin within a finite time under the adaptive observer (21).

Choose the Lyapunov function V_2

$$V_2 = \frac{1}{2} \tilde{D}^2 + \frac{1}{2} \tilde{\beta}_2^2. \quad (25)$$

By differentiating V_2 with respect to the equation (21), we obtain:

$$\begin{aligned} \dot{V}_2 &= \tilde{D}(\dot{\tilde{D}} - \dot{\tilde{\beta}}_2 \dot{\tilde{\beta}}_2) - \tilde{\beta}_2 \dot{\tilde{\beta}}_2 \\ &= -\lambda_1 \tilde{D}^2 + \tilde{D} \dot{\tilde{D}} - (\hat{\beta}_2 + \lambda_2) \tilde{D} \operatorname{sgn}(v) \\ &\quad - \tilde{\beta}_2 (-\lambda_3 \hat{\beta}_2 + |v|). \end{aligned} \quad (26)$$

When time $t > t_1$ $s = \dot{s} = 0$ holds, and at this point, $\tilde{D} = v$. Thus, the equation (26) can be rewritten as

$$\begin{aligned} \dot{V}_2 &\leq \beta_2 \tilde{D} - \hat{\beta}_2 |\tilde{D}| - \lambda_2 |\tilde{D}| + \lambda_3 \hat{\beta}_2 \tilde{\beta}_2 - \tilde{\beta}_2 |\tilde{D}| \\ &\leq -\lambda_2 |\tilde{D}| + \lambda_3 \hat{\beta}_2 \tilde{\beta}_2 \end{aligned} \quad (27)$$

Since $2\beta_2 \tilde{\beta}_2 \leq \beta_2^2 - \tilde{\beta}_2^2$ and $4|\tilde{\beta}_2| \leq 4\tilde{\beta}_2^2 + 1$ always hold, so

$$\begin{cases} 2\hat{\beta}_2 \tilde{\beta}_2 = 2\tilde{\beta}_2 (\beta_2 - \tilde{\beta}_2) \leq \beta_2^2 - \tilde{\beta}_2^2 \\ \beta_2^2 - \tilde{\beta}_2^2 + |\tilde{\beta}_2| \leq \beta_2^2 - \tilde{\beta}_2^2 + \tilde{\beta}_2^2 + \frac{1}{4} = \beta_2^2 + \frac{1}{4} \end{cases} \quad (28)$$

Thus, the equation (27) can be rewritten as

$$\begin{aligned} \dot{V}_2 &\leq -\lambda_2 |\tilde{D}| + \frac{\lambda_3}{2} \left(\beta_2^2 - \tilde{\beta}_2^2 + |\tilde{\beta}_2| - |\tilde{\beta}_2| \right) \\ &\leq -\lambda_3 |\tilde{D}| + \frac{\lambda_3}{2} \left(\beta_2^2 - |\tilde{\beta}_2| + \frac{1}{4} \right) \\ &\leq -\min \left\{ \lambda_2, \frac{\lambda_3}{2} \right\} \left(|\tilde{D}| + |\tilde{\beta}_2| \right) + \frac{\lambda_3}{2} \left(\beta_2^2 + \frac{1}{4} \right) \\ &= -\vartheta V_2^{\frac{1}{2}} + o \end{aligned} \quad (29)$$

where $\vartheta = \min \left\{ \lambda_2, \frac{\lambda_3}{2} \right\}$, $o = \frac{\lambda_3}{2} \left(\beta_2^2 + \frac{1}{4} \right)$

By combining equation (29) with Lemma 2, the convergence range of the estimation error \tilde{D} can be obtained as

$$|\tilde{D}| \leq \frac{o}{(1 - \theta_0)\vartheta}. \quad (30)$$

And the convergence time of the estimated error is \tilde{D}

$$t_2 = \frac{2V_2^{1/2}(t_0 + t_1)}{\theta_0\vartheta}. \quad (31)$$

In conclusion, the proposed nested adaptive observer (21) guarantees that the observation error \tilde{D} converges to a neighborhood around the origin within a finite time, with the final convergence time given by

$$t_3 = t_0 + t_1 + t_2. \quad (32)$$

Proof completed. \square

Remark 2. The adaptive law can effectively adapt to the disturbance variations. In fact, after $s = 0$, the third equation in (21) equals to

$$\dot{\hat{\beta}}_2 = -\lambda_3\hat{\beta}_2 + |\tilde{D}|. \quad (33)$$

Equation (33) is employed to estimate the upper bound of the disturbance derivative, whose dynamic characteristics are jointly determined by the parameter λ_3 and the estimation error $|\tilde{D}|$. The magnitude of $|\tilde{D}|$ directly influences the growth rate of $\hat{\beta}_2$: a larger $|\tilde{D}|$ accelerates the increase of $\hat{\beta}_2$, whereas as $|\tilde{D}|$ approaches zero, $\hat{\beta}_2$ exhibits an exponential decay with a rate governed by λ_3 . The selection of λ_3 imposes a dual effect on system performance: while increasing λ_3 enhances the convergence speed of $\hat{\beta}_2$, thereby reducing the convergence time of the estimator $|\tilde{D}|$, an excessively large λ_3 may diminish the system's sensitivity to the estimation error $|\tilde{D}|$, potentially degrading estimation accuracy. Consequently, λ_3 must be carefully chosen in practical applications to achieve an optimal trade-off between convergence speed and estimation precision.

To address this issue, by combining equations (29) and (30), let $\lambda_3 \leq 2\lambda_2$, so $\vartheta = \lambda_3$, then:

$$|\tilde{D}| \leq \frac{4\beta_2^2 + 1}{8(1 - \theta_0)}. \quad (34)$$

It is independent of λ_2 and λ_3 . Therefore, larger values of λ_2 and λ_3 can be chosen to reduce the convergence time without sacrificing estimation accuracy.

Theorem 2. Under the designed ADO, the estimated disturbance and observation error D always remain within the following allowable range:

$$|\hat{D}| \leq \lambda_p, |\tilde{D}| \leq \lambda_d \quad (35)$$

$$\begin{cases} \lambda_p = |\hat{D}(0)| + \frac{\lambda_2}{\lambda_1} + \beta_1 + \left| \frac{\hat{\beta}_2(0)}{\lambda_1} \right| + \frac{M + \bar{\delta}}{\lambda_1 \lambda_3} \\ \lambda_d = |\tilde{D}(0)| + \left| \beta_2 - \lambda_2 - \hat{\beta}_2(0) - \frac{M + \bar{\delta}}{\lambda_3} \right| \frac{1}{\lambda_1} \end{cases} \quad (36)$$

Specifically, λ_p and λ_d denote the upper bounds of \hat{D} and \tilde{D} , respectively, while $\hat{D}(0)$, $\tilde{D}(0)$ and $\hat{\beta}_2$ representing the initial values of \hat{D} , \tilde{D} and $\hat{\beta}_2$, respectively.

Proof. By solving the differential equation (21)

$$\begin{aligned} \hat{\beta}_2 &= \hat{\beta}_2(0)e^{-\lambda_3 t} + e^{-\lambda_3 t} \int_0^t |v| e^{\lambda_3 s} ds \\ &\leq \hat{\beta}_2(0)e^{-\lambda_3 t} + (M + \bar{\delta})e^{-\lambda_3 t} \int_0^t e^{\lambda_3 s} ds \\ &\leq \hat{\beta}_2(0) + \frac{M + \bar{\delta}}{\lambda_3}. \end{aligned} \quad (37)$$

Differentiate \hat{D} in equation (21) and substitute the remaining equations into it

$$\begin{aligned} \dot{\hat{D}} &= -\lambda_1(u + \hat{D}) + \text{sgn}(v)(\hat{\beta}_2 + \lambda_2) + \lambda_1 m_{s0} \dot{x}_2 \\ &= -\lambda_1 \hat{D} + \lambda_1 D + \text{sgn}(v)(\hat{\beta}_2 + \lambda_2) \end{aligned} \quad (38)$$

Derived by solving differential equation (38)

$$\begin{aligned} \hat{D} &= \hat{D}(0)e^{-\lambda_1 t} + e^{-\lambda_1 t} \int_0^t \left((\hat{\beta}_2 + \lambda_2) \text{sgn}(v) + \lambda_1 D \right) e^{\lambda_1 s} ds \\ &\leq \hat{D}(0)e^{-\lambda_1 t} + \frac{\lambda_2}{\lambda_1} + \beta_1 + \left(\left| \hat{\beta}_2(0) \right| + \frac{M + \bar{\delta}}{\lambda_3} \right) \frac{1}{\lambda_1} \\ &\rightarrow |\hat{D}| \leq |\hat{D}(0)| + \left(\frac{\lambda_2}{\lambda_1} + \beta_1 + \frac{|\hat{\beta}_2(0)|}{\lambda_1} + \frac{M + \bar{\delta}}{\lambda_1 \lambda_3} \right) \\ &\leq \lambda_p \end{aligned} \quad (39)$$

According to equation (38), it can be obtained that

$$\dot{\tilde{D}} = -\lambda_1 \tilde{D} + \dot{D} - (\hat{\beta}_2 + \lambda_2) \text{sgn}(v). \quad (40)$$

Similarly, by solving the differential equation (40), it is derived that

$$\begin{aligned} \tilde{D} &= \tilde{D}(0)e^{-\lambda_1 t} + e^{-\lambda_1 t} \int_0^t \left(\dot{D} - (\hat{\beta}_2 + \lambda_2) \text{sgn}(v) \right) e^{\lambda_1 s} ds \\ &\leq \tilde{D}(0)e^{-\lambda_1 t} + \left(\beta_2 - \lambda_2 - \hat{\beta}_2(0) - \frac{M + \bar{\delta}}{\lambda_3} \right) \frac{1}{\lambda_1} \\ &\rightarrow |\tilde{D}| \leq |\tilde{D}(0)| + \left| \beta_2 - \lambda_2 - \hat{\beta}_2(0) - \frac{M + \bar{\delta}}{\lambda_3} \right| \frac{1}{\lambda_1} \\ &\leq \lambda_d \end{aligned} \quad (41)$$

By synthesizing the results of equation (41), we conclude that Theorem 2 is proven. \square

3.3. DEI

As highlighted in [34], disturbances can exhibit dual characteristics. When the direction of a disturbance coincides with the

intended motion direction, it may improve control performance. Consequently, investigating the interplay between disturbance effects, system stability, and control performance is crucial. To tackle this, a new DEI is introduced in this study, designed to leverage advantageous disturbances while reducing chattering effects.

Definition 1: For an active suspension system, the DEI is formulated defined as follows:

$$P = \frac{\hat{D}e}{|\hat{D}e| + \varepsilon} \quad (42)$$

ε is a relatively small positive constant.

If $e\hat{D} > 0$, it follows that $P > 0$, and vice versa. Therefore, the consistency between the state e and the direction of the disturbance estimation \hat{D} is reflected by equation (42). Accordingly, it can be concluded that $P < 0$ indicates that the disturbance characteristics are beneficial, $P > 0$ indicates that the disturbance characteristics are harmful, and $P = 0$ indicates that the disturbance has no effect.

SLF.

When the directional evaluation method DEI (42), as defined in Definition 1, is applied, the lumped disturbances acting on the active suspension system can be classified into beneficial, neutral, or harmful characteristics. When beneficial disturbances are detected, they can be retained in the controller to conserve energy and enhance control performance. Therefore, the following equation can be used to determine whether the lumped disturbances should be eliminated or retained during the control process,

$$H(P) = \begin{cases} 1 & P > 0 \\ (P + \varpi)^2 / \varpi^2 - \varpi < P < 0 \\ 0 & P < -\varpi \end{cases} \quad (43)$$

ϖ is a constant

Remark 3. It should be noted that the DEI is constructed based on the estimated disturbance \hat{D} , rather than the actual disturbance D , because the actual disturbance D is typically uncertain or unknown in practical applications. Based on this, even if the sign of the estimated disturbance \hat{D} contains errors during certain time intervals, the designed controller can still effectively maintain its tracking performance and system stability.

Remark 4. In [34–37], the DCI is defined as $P = \text{sgn}(e\hat{D})$. When $P > 0$, $H(P) = 1$ indicates that the disturbance is harmful; when $P < 0$, $H(P) = -1$ indicates that the disturbance is beneficial, and the controller can effectively utilize the disturbance. However, it should be noted that due to the introduction of the sign function, the value of P is restricted to discrete values $\{-1, 0, 1\}$, while $H(P)$ can only take discrete values $\{0, 1\}$. When the function $e\hat{D}$ fluctuates near zero, the values of P and $H(P)$ may change frequently, leading to chattering phenomena. To address this issue, this paper proposes a new method that introduces a continuous DCI to mitigate chattering effects.

3.4. Design of sliding mode controller

Define the system state error as

$$e = z_s - z_{sr}. \quad (44)$$

The expression for constructing the sliding mode surface σ is given as

$$\sigma = k\dot{e} + e \quad (45)$$

where $k > 0$ is the control parameter to be designed.

For the active suspension system, the PD-SMC method is designed as follows:

$$u = -k_p e - k_d \dot{e} - k_l \text{sgn}(\sigma) + m_{s0} \ddot{z}_{sr} - H(P) \hat{D} \quad (46)$$

where k_p, k_d, k_l are positive control gains. To better understand the controller design process, the entire control system is illustrated in figure 2.

Theorem 3: For the active suspension system (4), the control laws (40), (41), and (44) ensure that the sprung mass displacement z_s accurately tracks the desired trajectory z_{sr} , that is

$$\lim_{x \rightarrow \infty} e = 0, \lim_{x \rightarrow \infty} \dot{e} = 0 \quad (47)$$

provided that the following conditions are satisfied:

$$\begin{cases} k_l > \lambda_d - \lambda_p \\ kk_d > m_{s0} \end{cases}. \quad (48)$$

Proof. First, the Lyapunov function V_3 is introduced

$$V_3 = [e \dot{e}] L \begin{bmatrix} e \\ \dot{e} \end{bmatrix} + \frac{1}{2} \lambda k_p e^2 \quad (49)$$

$$L = \begin{pmatrix} k_d & m_{s0} \\ m_{s0} & km_{s0} \end{pmatrix} \quad (50)$$

where L is positive definite, hence V_3 is also positive definite. By substituting an equation (50) into an equation (49) and taking its derivative, we obtain

$$\begin{aligned} \dot{V}_3 &= [e \dot{e}] \begin{bmatrix} k_d & m_{s0} \\ m_{s0} & km_{s0} \end{bmatrix} \begin{bmatrix} \dot{e} \\ \ddot{e} \end{bmatrix} + kk_p e \dot{e} \\ &= \sigma \left(\tilde{D} - \hat{D} (1 - H(P)) \right) \\ &\quad - k_l |\sigma| - k_p e^2 - (kk_d - m_{s0}) \dot{e}^2 \\ &\leq |\sigma| (\lambda_d - \lambda_p - k_l) - k_p e^2 - (kk_d - m_{s0}) \dot{e}^2 \\ &\leq 0 \end{aligned} \quad (51)$$

Since the selected Lyapunov function V_3 is positive definite and its time derivative \dot{V}_3 is negative definite, it can be proven, based on the control methods designed in (42), (43), and (46), the active suspension system described in equation (4) is stable. Moreover, the sliding mode surface σ will asymptotically converge to zero, that is

$$\lim_{t \rightarrow \infty} \sigma = 0. \quad (52)$$

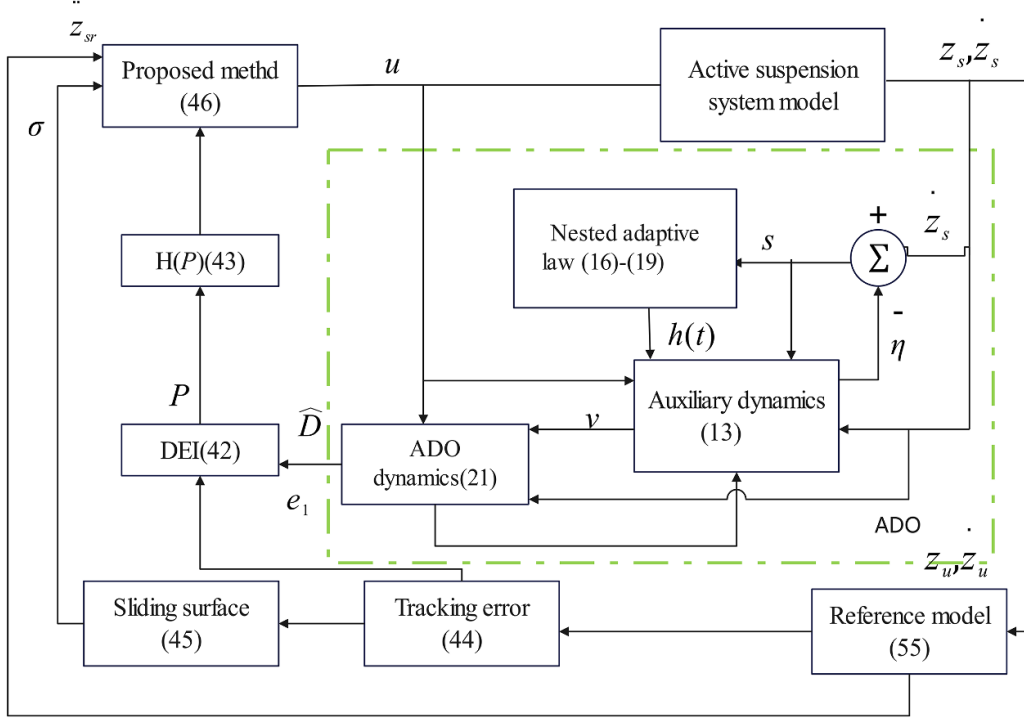


Figure 2. Block diagram for the overall control system.

When $\sigma = 0$, it follows from (45), it is derived that

$$e + k\dot{e} = 0. \quad (53)$$

By solving the differential equation (53), it is calculated that

$$e = c_1 e^{-\frac{1}{k}t}, \dot{e} = -\frac{1}{k}c_1 e^{-\frac{1}{k}t} \rightarrow \lim_{t \rightarrow \infty} e = 0, \lim_{t \rightarrow \infty} \dot{e} = 0 \quad (54)$$

where c_1 represents an arbitrary constant.

In summary, theorem three is proved. \square

3.5. Control parameter selection

(1) The selection of the values for $\tau, \delta_0, r_0, \alpha_1, \alpha_2$ and μ is as follows: τ represents the time constant of the low-pass filter (19), where a smaller τ indicates faster estimation speed. A smaller δ_0 will drive the system to reach the safety margin more quickly; however, its value should be greater than the influence range of noise or computational errors to avoid unnecessary oscillations or error amplification [45]. As mentioned earlier, the upper bound l of the disturbance in inequality (20) is unknown. To satisfy (20), a sufficiently large μ can be selected to mitigate the effect of l . In the experiments, the parameters r_0 and α_1 ($0 < \alpha_1 < 1$) have minimal impact on the convergence performance of the algorithm, an overlarge value of α_2 might lead to system instability [43]. In our case, we choose: $\tau = 0.016$, $\delta_0 = 0.001$, $r_0 = 1$, $\alpha_1 = 0.99$, $\alpha_2 = 1$, $\mu = 100$, $\lambda_0 = 5$, $\bar{\delta} = 0.01$.

(2) The selection of values for the disturbance observer is as follows: Larger values of λ_1, λ_2 and λ_3 result in faster convergence of the estimation error \tilde{D} . However, if λ_3 becomes

excessively large, it may lead to increased estimation errors. According to remark 2 with $\lambda_3 = 2\lambda_2$, sensitivity analysis was conducted. The results indicate that $\lambda_1, \lambda_2 \in [0, 10]$ are crucial for stable operation. Appropriate gain values can reduce the impact of external disturbances and enhance the system's robustness. To optimize the gain parameters, a genetic algorithm [46] was employed for global optimization. The optimization results showed that the optimal gain parameters were $\lambda_1 = 10$, $\lambda_2 = 3$, and $\lambda_3 = 6$, at which point the system's stability and robustness were maximized.

(3) In this study, the following parameter values are chosen: The selection of values for k_p, k_d, k_l and k is as follows: A larger gain k results in faster convergence of the system state on the sliding mode surface σ , but it may lead to higher control energy consumption and increased oscillations. The selection of k_p and k_d primarily depends on the dynamic characteristics of the system. Generally, increasing k_p can improve the system's response speed while increasing k_d enhances system stability and reduces oscillations. The choice of k_l depends on the robustness requirements of the system. Typically, selecting a larger k_l can improve the response speed of the sliding mode control, but overly large gains should be avoided to prevent unnecessary high-frequency oscillations. In this study, the parameters optimized through the genetic algorithm were selected as $k_p = 10, k_d = 5, k_l = 1$, and $k = 4$, ensuring the optimal performance of the system.

3.6. Reference track

In [1–6], the control objective of the suspension system is achieved by driving the displacement of the sprung mass to zero. However, under certain conditions, such as when road

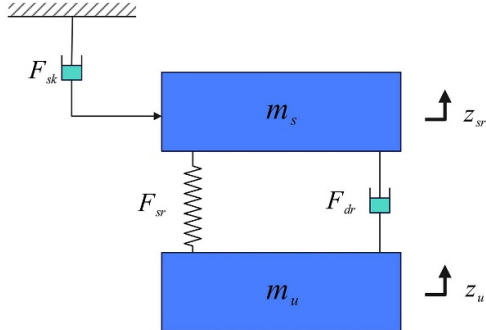


Figure 3. Skyhook damping model.

Table 1. Active suspension system and reference model parameter.

Argument	Numerical values		Numerical values		Units
	Units	Parameters	Units	Parameters	
m_s	2.45	kg	m_u	1	kg
k_s	980	$N\ m^{-1}$	k_{us}	2500	$N\ m^{-1}$
c_s	7.5	$Ns\ m^{-1}$	c_{us}	5	$Ns\ m^{-1}$
k_2	800	$N\ m^{-1}$	c_2	7.5	$Ns\ m^{-1}$
c_{sk}	120	$Ns\ m^{-1}$	t_{max}	0.0045	m
z_{max}	0.038	m			

irregularities exceed the operational range of the suspension system, this method may not meet the system's performance requirements. To overcome this limitation, a skyhook model (depicted in figure 3) can be employed to generate the reference trajectory for the vehicle body displacement [47], enhancing the system's adaptability and performance. The mathematical representation of this model is given as follows:

$$m_s \ddot{z}_{sr} + F_{sr} + F_{dr} + F_{sk} = 0 \quad (55)$$

$$\begin{cases} F_{sk} = c_{sk} \dot{z}_{sr} \\ F_{dr} = c_2 (\dot{z}_{sr} - \dot{z}_u) \\ F_{sr} = k_2 (z_{sr} - z_u) \end{cases} \quad (56)$$

where z_{sr} represents the sprung mass displacement in the skyhook model; F_{sr} , F_{dr} , and F_{sk} correspond to the suspension spring force, the damping force of the damper, and the skyhook damping force, respectively. The parameters of the skyhook damping model are provided in table 1.

4. Comparative experimental studies

4.1. Experimental platform

This section validates the proposed controller using a quarter-car active suspension experimental setup and compares the experimental results with those of passive suspension systems and other controllers. The experimental results primarily illustrate the performance of each controller in trajectory tracking and body acceleration suppression, particularly under random road disturbance conditions.

The experimental setup, shown in figure 4, simulates the sprung mass, unsprung mass, and road conditions using three

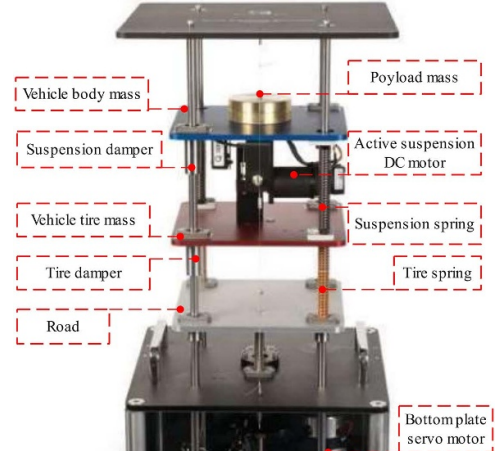


Figure 4. Active suspension setup.

Table 2. Controller gain.

Controller	Gain
SMC-DO-SM controller	$d_1 = 4, d_2 = 1, q = 100, l = 0.5, \varepsilon = 0.015, k = 5,$
SPD-SMC controller	$K_p = 50, K_d = 50, K_s = 10, \lambda = 20$
Proposed controller	$k_p = 10, k_d = 5, k_l = 1, k = 4$

plates. The blue plate represents the sprung mass and includes adjustable dead weights. The red plate corresponds to the unsprung mass. Suspension springs, dampers, and rotary DC motor actuators are positioned between the blue and red plates. At the base, DC motors generate signals to move the white plate, mimicking uneven road surfaces. A 10-bit optical encoder measures the positions of the blue and red plates, while an accelerometer records acceleration data. The velocity of the sprung mass is derived by processing position data through a high-pass filter. It is important to note that the control strategy does not require the position, velocity, or acceleration of the unsprung mass. Thus, control implementation relies solely on encoder measurements to determine the position of the blue plate. In the experimental setup, all system states are accessible. Additionally, while the setup approximates a linear system, it may include minor unmodeled dynamics and nonlinearities.

For better comparison, consider the following five scenarios. The control gains of the other three controllers are recorded in table 2.

- (1) Passive: this abbreviation is the passive suspension.
- (2) SPD-SMC: this abbreviation means the saturated PD with sliding mode control [25];
- (3) SMC-DO: this abbreviation denotes disturbance observer-based sliding mode control [32];

- (4) Proposed-t: This abbreviation refers to the control method designed in this paper, which combines the traditional DEI such as [39];
- (5) Proposed: this abbreviation indicates the control method designed in this paper, which is shown in the formula (44).

It is important to note that the primary distinction between Proposed-t and Proposed is observed in the control power, while their performance in other metrics remains comparable. As a result, the experimental outcomes for Proposed-t are presented exclusively through the control power plot, without the need for redundant presentation of other similar data.

4.2. Experimental results and analysis

Case 1: bump road.

To assess the control performance of the aforementioned controllers, a single disturbance event, characterized by high intensity and short duration as described in [24], is chosen as the road input. This disturbance is represented by the following equation:

$$z_r = \begin{cases} Sh \left(1 - \cos \left(\frac{\pi v_b t}{L} \right) \right), & \text{for } 0 \leq t \leq \frac{L}{v_b} \\ 0; & \text{otherwise} \end{cases} \quad (57)$$

where $h = 0.01\text{ m}$ is half the bump height, $v_b = 90\text{ km h}^{-1}$ is the vehicle velocity, $L = 5\text{ m}$ is the length of the bump, and $S = 0.5$ is a positive constant to ensure that the road excitation remains within the limits of the experimental setup. The experimental results are displayed in figure 5.

Case 2. Random road.

To further validate the performance of the aforementioned controllers in suppressing body acceleration, the performance of the suspension system under the conditions of a 40 km h^{-1} vehicle speed on a B-class road was investigated [29]. It should be noted that, to meet the constraints of the experimental setup, the amplitude of the random excitation was halved. The road profile is shown in figure 6 and the experimental results are presented in figure 7 through 12.

Figures 5(a) and 8 illustrate the body acceleration response curves of the passive suspension system, SPD-SMC controller, SMC-DO controller, and the proposed controller under bump and random road excitations, respectively. Table 3 summarizes the RMS values of body acceleration. Under bump road excitation, the RMS value of body acceleration (in meters per square second) for the passive suspension system is 0.4983, while the corresponding values for the three controllers are 0.2540, 0.2215, and 0.1612, respectively. Clearly, the proposed controller significantly reduces the RMS value of body acceleration, thus improving ride comfort. Under random road excitation, the results in figure 8 and table 3 show that the RMS values of body acceleration for the three active suspension systems are reduced by 3.00%, 36.24%, and 52.54%, respectively. Figure 9 presents the power spectral density of the body acceleration for the four suspension systems under random road disturbances. From the figure, it is evident that, within the mid-to-low frequency range, the proposed controller outperforms the other two controllers in suppressing body

acceleration. How-ever, the vibration isolation performance of all three active suspension systems, particularly the SMC-DO controller, deteriorates in the high-frequency range. Overall, the provided figures and data demonstrate that the proposed controller is a more effective approach, capable of effectively isolating disturbances and enhancing system performance.

Figures 5(b) and 7 illustrate the comparison of body displacement response performance between the proposed controller and the SMC-DO controller under bump and random road excitations, respectively. In figure 5(b), the proposed controller exhibits smaller oscillations and faster convergence when tracking the desired trajectory (RT) compared to the SMC-DO controller, particularly in the 0–0.5 s interval, where it more accurately follows the desired trajectory, significantly reducing unnecessary oscillations. Under random road excitation, as shown in figure 7, the proposed controller also demonstrates superior performance, with a smoother body displacement response and higher tracking accuracy, significantly reducing fluctuations. Compared to the SMC-DO controller, it more effectively suppresses the impact of external disturbances. Overall, the proposed controller shows stronger control capabilities in reducing high-frequency oscillations, improving tracking accuracy, and enhancing system stability and comfort.

Under both bump and random road conditions, the control input signals for the active suspension system are shown in figures 5(e) and 12, with table 4 summarizing the RMS values of the control inputs for various controllers. Under bump road excitation, the RMS value of the control force for the proposed controller is 0.9413, which is 34.79% lower than the SPD-SMC controller, 6.49% lower than the SMC-DO controller, and 12.54% lower than the Proposed-t controller. This indicates that the proposed controller effectively suppresses fluctuations by reducing the control force amplitude, significantly improving system stability. Under random road excitation, the RMS values of the control forces for the four controllers are 2.2235, 1.2742, 0.9190, and 1.0433, respectively. The proposed controller outperforms the others, demonstrating a more efficient control strategy.

Overall, the designed controller reduces high-frequency components and control input amplitude, significantly lowering energy consumption and actuator bandwidth requirements, while enhancing system stability and adaptability, making it more suitable for practical applications.

Figures 5(c) and 10 illustrate the suspension deflection for four suspension systems, while figures 5(d) and 11 show the tire deflection for the same systems, with relevant evaluation metrics summarized in table 5. Under bump road excitation, all three active suspension controllers significantly outperform the passive suspension system in terms of the maximum relative suspension displacement (MRSD). However, under random road excitation, the MRSD performance of the active suspensions shows a relative deterioration. This is primarily due to the broadband characteristics and non-stationary nature of the random excitation, which challenges the tracking accuracy of the control system.

In terms of tire deflection, under bump excitation, the maximum relative tire displacement (MRTD) of the three active

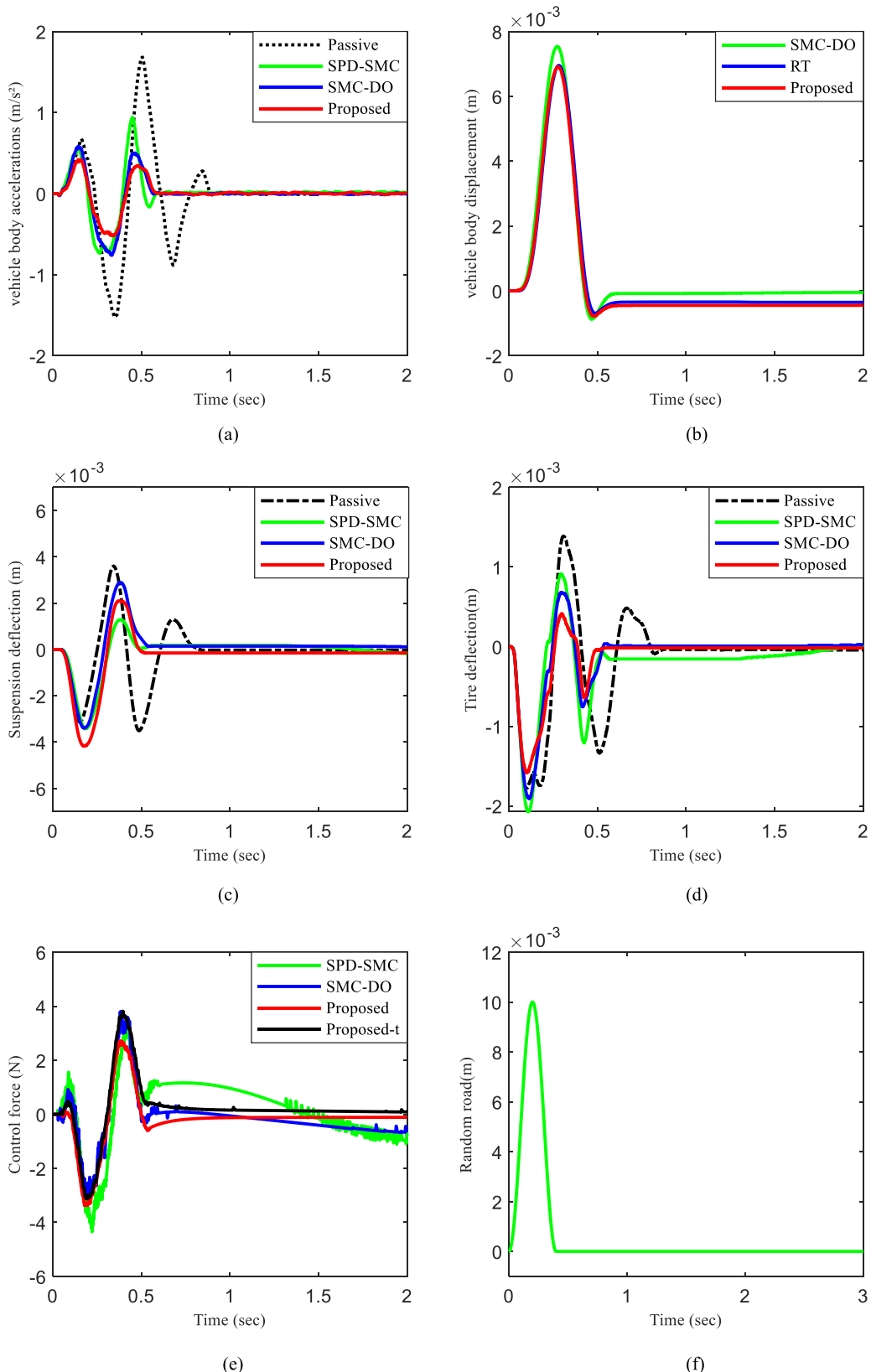
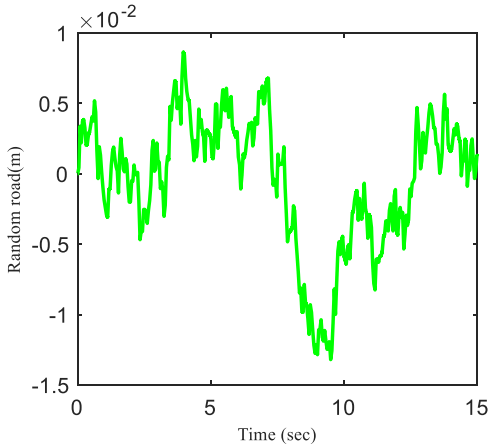
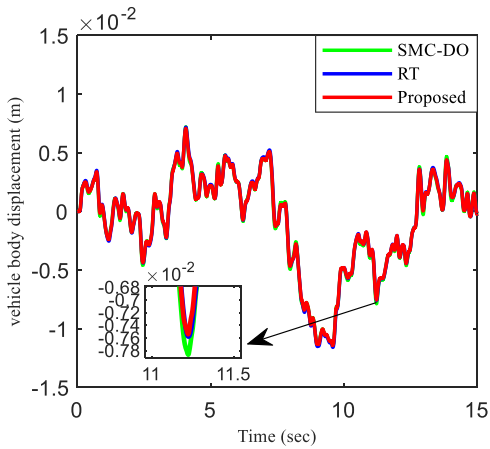


Figure 5. Experimental result with bump road: (a) vehicle body acceleration; (b) vehicle body displacement; (c) suspension deflection; (d) tire deflection; (e) control input; (f) the bump road profile.

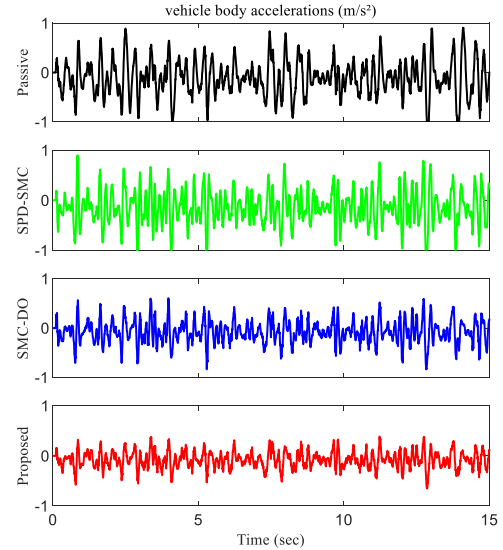
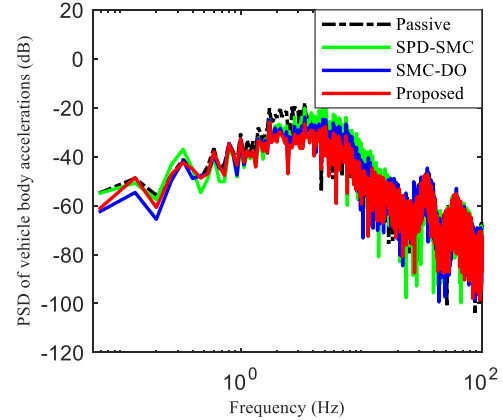
**Figure 6.** Random road profile.**Figure 7.** The vehicle body displacement for random road.

suspension controllers improves compared to the passive suspension system. However, under random road conditions, the MRTD performance also exhibits a decline. This performance degradation can be attributed to the irregularities and abrupt characteristics of the random road excitation, which make it difficult for the control system to respond accurately and promptly, thereby extending the system's response delay time.

It should be noted that although both metrics show performance degradation under random road conditions, the measured MRSD and MRTD values remain consistently below 1 for all road excitations. Therefore, the suspension deflections and tire deflections for all three suspensions stay within the safety threshold. This indicates that the designed tracking controller effectively ensures the driving safety of both the driver and passengers.

5. Simulation analysis

To further verify the effectiveness of the designed controller, a simulation model of the half-vehicle active suspension was established. The relevant parameters of the active suspension are listed in table 7,

**Figure 8.** Vehicle body acceleration for random road profile.**Figure 9.** PSD of vehicle body acceleration for random road profile.

$$\begin{cases} M_s \ddot{Z}_c + F_{cf} + F_{dr} + F_{sf} + F_{sr} = u_z \\ I\psi_c + a(F_{df} + F_{sf}) - b(F_{dr} + F_{sr}) = u_\psi \\ m_f \ddot{Z}_{wf} - F_{sf} - F_{df} + F_{tf} + F_{bf} = -u_f \\ m_r \ddot{Z}_{wr} - F_{sr} - F_{dr} + F_{tr} + F_{br} = -u_r \end{cases} \quad (58)$$

where $u_z = u_f + u_r$ and $u_\psi = au_f - bu_r$.

When considering the inherent nonlinearity of the spring, the forces generated by the suspension system and the tire follow the following equations:

$$\begin{cases} F_{si} = k_{i1}(Z_i - Z_{wi}) + k_{ni1}(Z_i - Z_{wi})^3 \\ F_{di} = b_{ej}(\dot{Z}_i - \dot{Z}_{wi}) \\ F_{ti} = k_{i2}(Z_{wi} - Z_{ri}) \\ F_{bi} = b_{i2}(\dot{Z}_{wi} - \dot{Z}_{ri}) \end{cases} \quad (59)$$

Here, for $i = f$ (front), $j = 1$ and for $i = r$ (rear), $j = 2$. Z_f and Z_r are displacements of sprung mass given by

$$\begin{cases} Z_f = Z_c + a \sin \psi \\ Z_r = Z_c - b \sin \psi \end{cases} \quad (60)$$

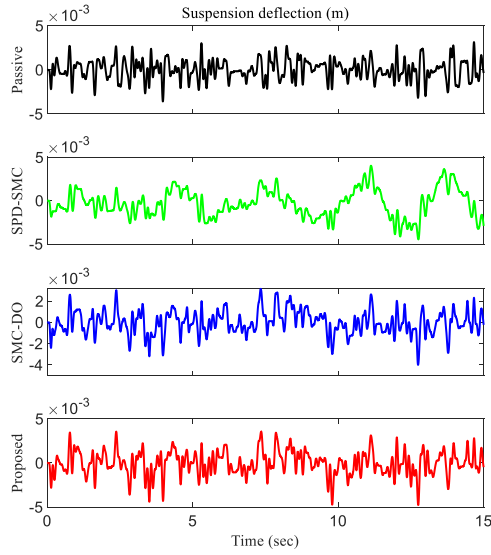


Figure 10. Suspension deflection for random road profile.

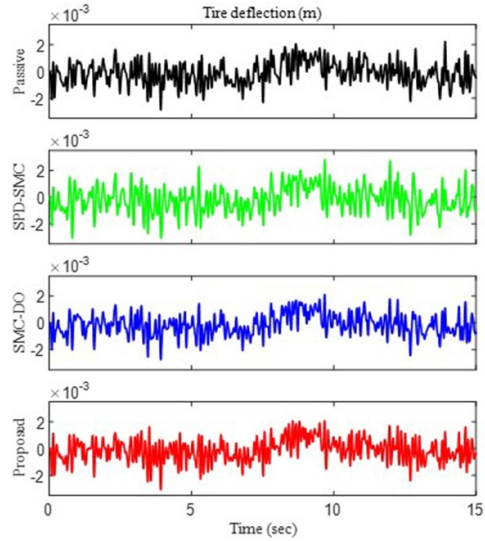


Figure 11. Tire deflection for random road profile.

k_{il} and k_{nil} are the stiffness coefficients of the linear and nonlinear term respectively; b_{ej} is the damping coefficients; k_{i2} and b_{i2} are the stiffness and damping coefficient of tires, respectively.

Due to the uncertainties in the model parameters of the half-car system considered in equation (58) and the influence of external disturbances, the dynamic equations for the vertical motion and pitching motion of the sprung mass can be rewritten as:

$$\begin{cases} \ddot{Z}_c = \frac{1}{M_n} (-F_{zn} + u_z) + D_1 \\ \ddot{\psi}_c = \frac{1}{I_n} (-F_{\psi n} + u_{\psi}) + D_2 \end{cases} \quad (61)$$

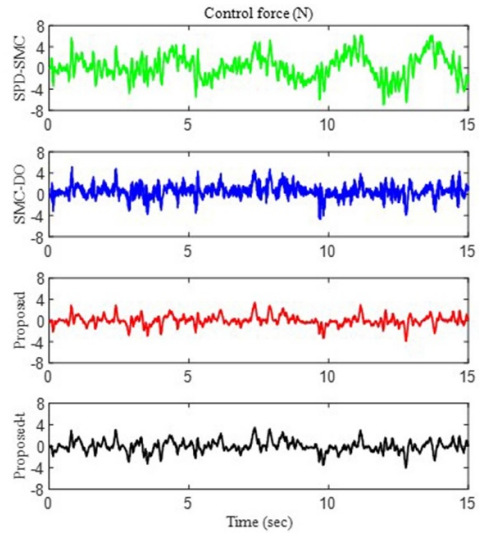


Figure 12. Control force for random road profile.

where

$$\begin{cases} F_{zn} = k_{f10}Z_f + k_{r10}Z_r + b_{ef0}\dot{Z}_f + b_{er0}\dot{Z}_r \\ D_1 = \frac{1}{M_n}(F_{zn} - u_z) - \frac{1}{M}(F_{df} + F_{dr} + F_{sf} + F_{sr} - u_z) \\ F_{\psi n} = -a(b_{ef0}\dot{Z}_f + k_{f10}Z_f) + b(b_{er0}\dot{Z}_r + k_{r10}Z_r) \\ D_2 = \frac{1}{I_n}(F_{\psi n} - u_{\psi}) - \frac{1}{I}(-a(F_{df} + F_{sf}) + b(F_{dr} + F_{sr}) - u_{\psi}) \end{cases} \quad (62)$$

M_n, I_n are nominal values of mass and moment of inertia of vehicle body; k_{fn}, k_{rn} are the nominal values of front and rear suspension spring; b_{fn} and b_{rn} are the nominal values of damping coefficient of front and rear suspension respectively.

The control force is designed in the following manner to ensure the stability and performance of the system,

$$\begin{cases} u_z = F_{zn} - k_{p1}z_c - k_{d1}\dot{z}_c - k_{l1}\operatorname{sgn}(\sigma) - H(P)\hat{D}_1 \\ u_{\psi} = F_{\psi n} - k_{p2}z_c - k_{d2}\dot{z}_c - k_{l2}\operatorname{sgn}(\sigma) - H(P)\hat{D}_2 \end{cases} \quad (63)$$

\hat{D}_1 and \hat{D}_2 are derived through the adaptive observer proposed in the paper, aiming to achieve precise estimation and compensation of system disturbances.

The system parameters used for simulation are listed in table 6. The initial conditions of the plant are assumed to be zero, with the nominal values of suspension parameters taken as $M_{s0} = 1100\text{ kg}$, $I_0 = 550\text{ kg m}^2$, $b_{ef0} = b_{er0} = 1400\text{ N s m}^{-1}$.

$k_{f10} = 16000\text{ N m}^{-1}$, $k_{r10} = 14000\text{ N m}^{-1}$ [48]. The controller parameters are tuned and taken as $k_{p1} = k_{p2} = 10$, $k_{d1} = k_{d2} = 5$, $k_{l1} = k_{l2} = 1$.

The system response was tested under the road profile given by equation (57). Notice that $S = 2.5$ assuming that the road conditions for the front and rear wheels are the same, a time delay of $(a + b)/v_b$ exists, where v_b represents the vehicle speed, set at 90 km h^{-1} . To validate the effectiveness of the designed controller, a comparison is made with the passive suspension system. The system response results are shown in

Table 3. RMS of the vehicle body acceleration.

Controllers	Bump road		Random road	
	RMS (m s^{-2})	Reduction (%)	RMS (m s^{-2})	Reduction (%)
Passive	0.4983	0	0.3700	0
SPD-SMC controller	0.2540	49.03%	0.3660	3.000%
SMC-DO controller	0.2215	55.56%	0.2359	36.24%
Proposed controller	0.1612	67.67%	0.1756	52.54%

Table 4. Root mean square of control inputs for different controllers.

Controllers	Bump road	Random road
	Control force RMS (N)	Control force RMS (N)
SPD-SMC controller	1.2688	2.2235
SMC-DO controller	1.0024	1.2742
Proposed controller	0.9413	0.9190
Proposed-t controller	1.0593	1.0433

Table 5. MRSD and MRTD for different controllers.

Controllers	MRSD		MRTD	
	Bump road	Random road	Bump road	Random road
Passive	0.1390	0.1178	0.0320	0.6422
SPD-SMC controller	0.1120	0.1470	0.0222	0.6800
SMC-DO controller	0.0995	0.1313	0.0263	0.6111
Proposed controller	0.0850	0.1550	0.0296	0.7300

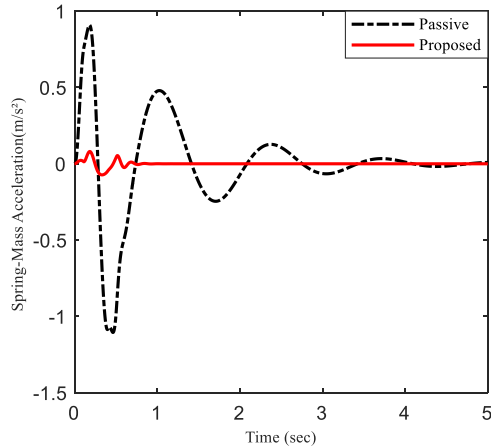
Table 6. Model parameter values.

Parameter	Value	Parameter	Value
M_s	1200 kg	I	600 kg m^2
m_f, m_r	100 kg	b_{e1}, b_{e2}	1500 Ns m^{-1}
k_{f1}, k_{r1}	15 000 N m^{-1}	b_{f2}	1500 Ns m^{-1}
k_{nf1}, k_{nr1}	1000 N m^{-3}	b_{r2}	2000 Ns m^{-1}
k_{f2}	200 000 N m^{-1}	a	1.2 m
k_{r2}	150 000 N m^{-1}	b	1.5 m

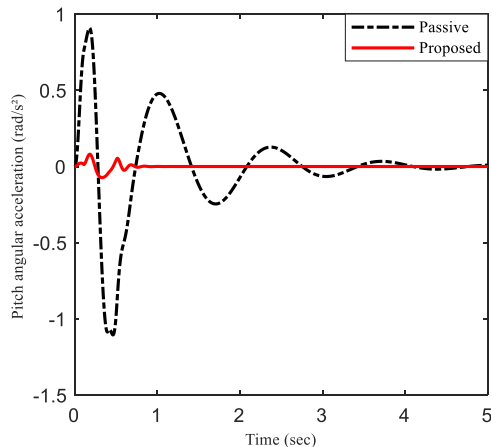
figures 13–15, with the relevant evaluation metrics summarized in table 7.

Based on the analysis presented in figures 13–15 and Table 7, it is evident that the proposed controller surpasses the passive suspension system across all primary performance metrics, particularly in terms of vibration damping, ride comfort, and handling performance. Specifically, the proposed controller achieves a substantial reduction in the RMS val-

of vertical acceleration and pitch angular acceleration, while effectively minimizing the displacement disparities between the front and rear suspension systems and tires. The controller demonstrates a marked improvement in controlling the maximum displacement differences. These findings suggest that the proposed controller delivers enhanced dynamic response and superior vehicle stability when subjected to road excitations, resulting in a significant enhancement in both ride comfort and handling capabilities.



(a)

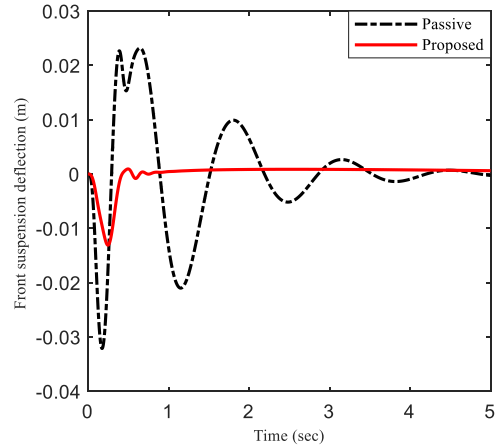


(b)

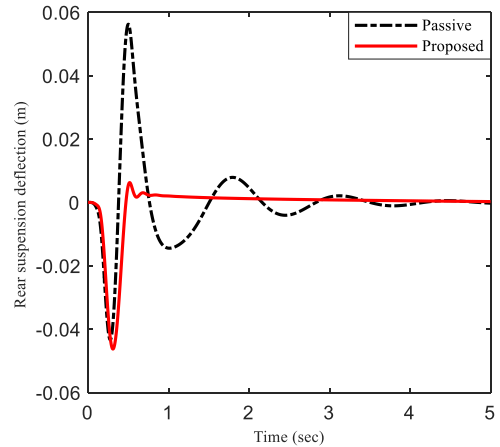
Figure 13. Simulation results of acceleration felt by vehicle body due to: (a) spring-mass acceleration (b) pitch angular acceleration.

6. Conclusion

To address the inherent uncertainties and external disturbances in active suspension systems, this study introduces proportional-derivative sliding mode control strategy combined with an ADO. To overcome the challenge of estimating system disturbances, an ADO is developed, which operates without requiring prior knowledge of disturbance bounds or their derivatives, ensuring that estimation errors converge within a finite time. Additionally, a new method for condition-based disturbance compensation has been designed to evaluate



(a)



(b)

Figure 14. Simulation results of suspension deflection: (a) front, (b) rear.

the disturbances compensated by the disturbance observer. This method includes a DCI and a SLF, which are capable of eliminating harmful disturbances while retaining beneficial ones. Experimental results show that, compared to the passive suspension system, the proposed controller reduces the RMS values of body acceleration by 67.67% and 52.54% under sinusoidal, random, and bump road conditions. Compared to the SPD-SMC and SMC-DO controllers, the proposed controller not only performs better in vibration suppression but also significantly reduces the RMS value of control inputs, improving vehicle ride comfort and reducing energy consumption.

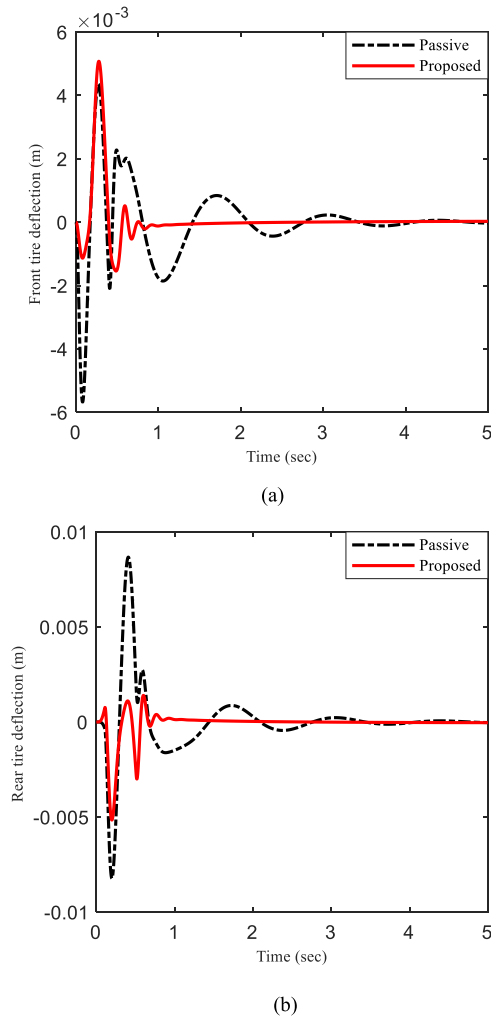


Figure 15. Simulation results of tire deflection: (a) front, (b) rear.

Table 7. Model parameter values summary of simulation results for the bump road profile.

Measures	Passive	Proposed
RMS (\ddot{Z}_c)	0.3054	0.0154
RMS ($\dot{\psi}_c$)	0.5782	0.0349
$\max z_f - z_{wf} $	0.0321	0.0131
$\max z_r - z_{wr} $	0.0562	0.0463
$\max z_{wf} - z_{rf} $	0.0057	0.0051
$\max z_{wr} - z_{rr} $	0.0087	0.0052

Data availability statement

The data cannot be made publicly available upon publication because they are owned by a third party and the terms of use prevent public distribution. The data that support the findings of this study are available upon reasonable request from the authors.

Acknowledgment

This work is supported by Natural Science Foundation of Shandong Province (ZR2022QA058).

References

- Ji G, Li S, Feng G, Li Z and Liu X 2024 A novel DNFS control strategy for vehicle semi-active suspension system *Meas. Sci. Technol.* **35** 126203
- Lee D, Jin S and Lee C 2023 Deep reinforcement learning of semiactive suspension controller for vehicle ride comfort *IEEE Trans. Veh. Technol.* **72** 327–39
- Pang L, Yue M, Qi G and Zhao X 2025 Switched control strategy based on preview-based MPC for active suspension of heavy-duty vehicle to improve ride comfort and roll stability *Meas. Sci. Technol.* **36** 036201
- Du M, Zhao D, Yang M and Chen H 2020 Nonlinear extended state observer-based output feedback stabilization control for uncertain nonlinear half-car active suspension systems *Nonlinear Dyn.* **100** 2483–503
- Liu Y and Chen H 2021 Adaptive sliding mode control for uncertain active suspension systems with prescribed performance *IEEE Trans. Syst. Man Cybern. Syst.* **51** 6414–22
- Yan G, Fang M and Xu J 2019 Analysis and experiment of time-delayed optimal control for vehicle suspension system *J. Sound Vib.* **446** 144–58
- Luis O, Rios H and Ahmed H 2022 Robust control for an active suspension system via continuous sliding-mode controllers *Eng. Sci. Technol. Int. J.* **28** 101026
- Yin Y, Luo B, Ren H, Fang Q and Zhang C 2022 Robust control design for active suspension system with uncertain dynamics and actuator time delay *J. Mech. Sci. Technol.* **36** 6319–27
- Li W, Xie Z and Zhao J 2019 Fuzzy finite-frequency output feedback control for nonlinear active suspension systems with time delay and output constraints *Mech. Syst. Signal Process.* **132** 315–34
- Li H, Zhang Z, Yan H and Xie X 2019 Adaptive event-triggered fuzzy control for uncertain active suspension systems *IEEE Trans. Cybern.* **49** 4388–97
- Zhang M, Jing X and Wang G 2022 Bioinspired nonlinear dynamics-based adaptive neural network control for vehicle suspension systems with uncertain/unknown dynamics and input delay *IEEE Trans. Ind. Electron.* **68** 12646–56
- Lin B, Su X and Li X 2019 Fuzzy sliding mode control for active suspension system with proportional differential sliding mode observer *Asian J. Control* **21** 264–76
- Wang G, Chadli M and Basin M V 2021 Practical terminal sliding mode control of nonlinear uncertain active suspension systems with adaptive disturbance observer *IEEE/ASME Trans. Mechatronics* **26** 789–97
- Bai R and Wang H 2021 Robust optimal control for the vehicle suspension system with uncertainties *IEEE Trans. Cybern.* **52** 9263–73
- Pang H, Wang Y and Zhang X 2019 Robust state-feedback control design for active suspension system with time-varying input delay and wheelbase preview information *J. Franklin Inst.* **356** 1899–923
- Cao Z, Zhao W and Hou X 2019 Multi-objective robust control for vehicle active suspension systems via parameterized controller *IEEE Access* **8** 7455–65
- Pang H, Zhang X and Chen J 2019 Design of a coordinated adaptive backstepping tracking control for nonlinear uncertain active suspension system *Appl. Math. Modell.* **76** 479–94
- Taghavifar H, Mardani A and Hu C 2019 Adaptive robust nonlinear active suspension control using an observer-based modified sliding mode interval type-2 fuzzy neural network *IEEE Trans. Intell. Syst.* **5** 53–62
- Li M, Li J, Li G and Xu J 2022 Analysis of active suspension control based on improved fuzzy neural network PID *World Electr. Veh. J.* **13** 226

- [20] Han S Y, Dong J F, Zhou J and Chen Y-H 2022 Adaptive fuzzy PID control strategy for vehicle active suspension based on road evaluation *Electronics* **11** 921
- [21] Wang J, Jin F, Zhou L and Li P 2019 Implementation of model-free motion control for active suspension systems *Mech. Syst. Signal Process.* **119** 589–602
- [22] Song Y, Zhao W, Liu Z, Han J and Dang Q 2025 Nonlinear sliding mode control of flying wing aircraft under wind disturbance *Meas. Sci. Technol.* **36** 026206
- [23] Du M, Zhao D, Yang B and Wang L 2018 Terminal sliding mode control for full vehicle active suspension systems *J. Mech. Sci. Technol.* **32** 2851–66
- [24] Rajendiran S and Lakshmi P 2020 Performance analysis of fractional order terminal SMC for the half car model with random road input *J. Vib. Eng. Technol.* **8** 687–1597
- [25] Zhang M, Jing X, Huang W and Li P 2022 Saturated PD-SMC method for suspension systems by exploiting beneficial nonlinearities for improved vibration reduction and energy-saving performance *Mech. Syst. Signal Process.* **179** 109376
- [26] Yuan S, Shao S, Zhang T, Nan Y, Ma C, Wu Y, Sun Z and Liu J 2025 Dual objective nonlinear PD sliding mode control based on a reference model for an active suspension system *Nonlinear Dyn.* **113** 1449–65
- [27] Hong L, Liu J, Zhang Q and Zhang B 2025 Disturbance compensation control method for improving waveform accuracy of controlled active seismic source *Meas. Sci. Technol.* **36** 056212
- [28] Guo L, Guo P, Guan L and Ma H 2024 Model predictive path tracking control of intelligent vehicles based on dual-stage disturbance observer under multi-channel disturbances *Meas. Sci. Technol.* **35** 106202
- [29] Pusadkar U S, Chaudhari S D, Shendge P D and Phadke S B 2019 Linear disturbance observer based sliding mode control for active suspension systems with non-ideal actuator *J. Sound Vib.* **442** 428–44
- [30] Waghmare D B, Asutkar V G and Patre B M 2024 Nonlinear disturbance compensator for active suspension systems with actuator saturation *Int. J. Dyn. Control* **12** 1817–28
- [31] Ho C M, Tran D T and Ahn K K 2021 Adaptive sliding mode control based nonlinear disturbance observer for active suspension with pneumatic spring *J. Sound Vib.* **509** 116241
- [32] Qin W, Shangguan W and Zhao K 2020 A research of sliding mode control method with disturbance observer combining skyhook model for active suspension systems *J. Vib. Control.* **26** 952–64
- [33] Rabiee H, Ataei M and Ekramian M 2019 Continuous nonsingular terminal sliding mode control based on adaptive sliding mode disturbance observer for uncertain nonlinear systems *Automatica* **109** 108515
- [34] Zhu Y, Qiao J and Guo L 2018 Adaptive sliding mode disturbance observer-based composite control with prescribed performance of space manipulators for target capturing *IEEE Trans. Ind. Electron.* **66** 1973–83
- [35] Guo Z, Guo J, Zhou J and Chang J 2019 Robust tracking for hypersonic reentry vehicles via disturbance estimation-triggered control *IEEE Trans. Aerosp. Electron. Syst.* **56** 1279–89
- [36] Sun J, Pu Z and Yi J 2019 Conditional disturbance negation based active disturbance rejection control for hypersonic vehicles *Control Eng. Pract.* **84** 159–71
- [37] Fang X et al 2023 Conditional disturbance compensation control for an overactuated manned submersible vehicle *IEEE Trans. Ind. Inf.* **20** 4828–38
- [38] Wang G, Jing H and Huang C 2021 Nonlinear disturbance observer-based control for active suspension system via disturbance estimation-triggered approach *J. Vib. Eng. Technol.* **9** 1373–86
- [39] Zhang M and Jing X 2021 Switching logic-based saturated tracking control for active suspension systems based on disturbance observer and bioinspired X-dynamics *Mech. Syst. Signal Process.* **155** 107611
- [40] Li D, Yu H, Tee K P, Wu Y, Ge S S and Lee T H 2021 On time-synchronized stability and control *IEEE Trans. Syst. Man Cybern.* **52** 2450–63
- [41] Wang H, Liu P X, Zhao X and Liu X 2019 Adaptive fuzzy finite-time control of nonlinear systems with actuator faults *IEEE Trans. Cybern.* **50** 1786–97
- [42] Na J, Huang Y, Wu X, Su S-F and Li G 2019 Adaptive finite-time fuzzy control of nonlinear active suspension systems with input delay *IEEE Trans. Cybern.* **50** 2639–50
- [43] Sun Z, Zheng J, Man Z, Fu M and Lu R 2019 Nested adaptive super-twisting sliding mode control design for a vehicle steer-by-wire system *Mech. Syst. Signal Process.* **122** 658–72
- [44] Pan H, Zhang G, Ouyang H and Mei L 2020 Novel fixed-time nonsingular fast terminal sliding mode control for second-order uncertain systems based on adaptive disturbance observer *IEEE Access* **8** 126615–27
- [45] Edwards C and Shtessel Y B 2016 Adaptive continuous higher order sliding mode control *Automatica* **65** 183–90
- [46] Sohail A 2023 Genetic algorithms in the fields of artificial intelligence and data sciences *Ann. Data Sci.* **10** 1007–18
- [47] Qin W, Liu F, Yin H and Huang J 2021 Constraint-based adaptive robust control for active suspension systems under the sky-hook model *IEEE Trans. Ind. Electron.* **69** 5152–64
- [48] Waghmare D B, Asutkar V G and Patre B M 2021 Extended disturbance observer based robust sliding mode control for active suspension system *Int. J. Dyn. Control* **9** 1681–94